Geophys. J. R. astr. Soc. (1971) **22,** 353–376.

Source Parameters of Earthquakes from Spectra of Rayleigh Waves

(Received 1970 September 10)

Agustin Udias*

Summary

A generalized form of the directivity function has been used to determine the length and the rupture velocity of four earthquakes with known vertical strike slip faulting. For body wave magnitudes between 5·7 and 7·0, the lengths vary from 18 to 35 km with a rupture velocity of $1{\cdot}5\,\mathrm{km\,s^{-1}}$. Seismic moments have been determined from the spectral amplitude densities and the theoretical response to a point source model. From these values, stress drops of 2 to 30 bars and average dislocations of 4 to 160 cm have been derived. The products of the average stresses acting at the fault by the seismic efficiency factor are of the order of 10^7 dyne cm^{-2} for all four earthquakes; this seems to indicate a minimum strength of the crust under horizontal shear stress of the same order.

Introduction

The most basic parameters of the source of an earthquake are those defining its location in space and time, namely: latitude and longitude of the epicentre, depth, and origin time. These parameters consider the focus of an earthquake as a point from which seismic waves are radiated. The size was measured first using the intensity scale on the basis of the subsequent damage; later, the concept of magnitude was introduced which represents a certain measurement of the energy radiated in the form of seismic waves. The study of the mechanism acting at the source added some other parameters to those already mentioned. Approximating the source by a system of forces acting at a point, these parameters are: the orientation of the forces, or equivalently that of the two possible planes of faulting, and the type of system, usually a single or double couple. Progress in the understanding of the dynamics of faulting and in the methods of analysis or seismic waves made possible the determination of other parameters which add more information about the source. These are the length and width of the surface of faulting, the maximum and average displacement or dislocation on that surface, the overall resulting moment, the average stress on the fault and the stress drop during faulting. It is assumed, then, that earthquakes are produced by a slip along a plane fault surface. This hypothesis is well supported, at least for shallow depth shocks. This study presents the determination of some of these parameters from the analysis of the amplitude spectral densities of Rayleigh waves.

* Present address: Departamento de Geofisica, Universidad de Madrid, Madrid, Spain.

Table 1

Location parameters

	Date	Origin time	Lat.	Long.	Depth
ALEUT	1966 July 4	18 33 36	51·7 N	179·9 E	13
NORAT1	1963 August 3	10 21 37	7·7 N	35·8 W	33
NORAT2	1963 November 17	00 48 03	7·6 N	37·4 W	33
AZORES	1966 July 4	12 15 28	37·5 N	24·8 W	33

Table 2

Fault plane solutions

	Plane *A*		Plane *B*		*X*		*Y*		*Z*		Reference
	ϕ	δ	ϕ	δ	ϕ	θ	ϕ	θ	ϕ	θ	
ALEUT	7	85 E	97	85 S	7	5	277	5	145	83	Stauder (1968)
NORAT1	11	86 W	102	80 S	11	10	102	4	222	78	Stauder & Bollinger (1966)
NORAT2	175	85 E	85	89 N	175	1	265	5	73	5	Udias & Baumann (1969)
AZORES	6	54 E	112	70 S	22	20	276	36	135	47	Banghar & Sykes (1969)

For the present analysis four earthquakes have been selected. Their locations, as taken from the U.S.C.G.S. Bulletin, are given in Table 1. Their fault plane solutions have been determined already and are given in Table 2. Nodal planes of *P* are given by their strike, measured clockwise from north, and their dip; the *X*, *Y*, *Z* axes (the two axes along which the forces are oriented and the null axis) are given by their trend and plunge. Three of the solutions are based on the combined analysis of the direction of the first motion of *P* and the polarization angle of *S*. For these, the nodal planes of *P* are well defined, and the *S* data correspond to a double couple source. The solution for the mechanism of the Azores earthquake is based only on *P* data.

The mechanism solutions for NORAT1, NORAT2 and ALEUT represent strike-slip faulting along either of two vertical planes striking approximately NS and EW. For AZORES one of the planes has a larger component of strike-slip motion than the other. Three of the earthquakes are located in the mid-Atlantic ridge. NORAT1 and NORAT2 are associated clearly with transform faults displacing the ridge (Sykes 1967). AZORES belongs to the so-called Azores–Gibraltar ridge and the relation of its mechanism to the tectonics of the region is less clear (Banghar & Sykes 1966). The fourth earthquake, ALEUT, belongs to the Rat Islands sequence that started with the shock of 1965 4 February; its mechanism has been interpreted as an arc–arc transform fault (Stauder 1968).

Magnitude

As magnitude is the most readily available parameter to represent the size of an earthquake, its relation to the other source parameters is of particular importance. If the accuracy of these relations is to be improved, magnitudes must be more carefully determined. Magnitude is in itself a quite gross estimate, and there are several different methods of determining it, not all of them equivalent. For teleseismic data

two different magnitudes, m_b and M_s, are defined from body and surface waves. Reported values of magnitude do not always specify to which type they correspond. For the same earthquake they may differ substantially as can be seen in Table 3. The data correspond to NORAT1 and NORAT2 and are taken from the B.C.I.S. Bulletin.

Table 3

Reported values of magnitude

NORAT2		NORAT1	
6·6	Uppsala	7·35	Matsushiro
6·5	Blue Mtn	7·2	Tulsa, Moskva
6¼–6½	Pasadena	7	Uppsala
6·3	Uinta	6·9	Pasadena, Praha
6·2	Copenhagen	6·6	Balboa Heights
6–6¼	Palisades	6·5	Stuttgart
6·1	Georgetown	6·3	Blue Mtn
6·0	Tonto Forest	6·1	USCGS
5·9	USCGS	6·0	Tonto Forest
5½–5¾	Bensberg	5·5	Cumberland
5·6	Kevo, Arequipa	5·4	State College
5·5	State College		
5·4	Longmire		
5·2	Stuttgart		
4·4	Wichita		

For the purpose of comparing with other focal parameters, magnitudes have been calculated for the four earthquakes, from body and surface waves using the formulas

$$m_b = \log\left(\frac{A}{T}\right) + \sigma(\Delta), \tag{1}$$

$$M_s = \log\left(\frac{A}{T}\right) + 1{\cdot}66\log\Delta + 3{\cdot}3. \tag{2}$$

The amplitude A, in microns, has been measured in both cases from the vertical component of long period instruments; for m_b the ground motion amplitude of the first cycle of the P wave is used, and for M_s the largest amplitude of the surface waves. T is the corresponding period, which for the surface waves is about 20 s. $\sigma(\Delta)$ is the standard calibration function as given by Karnik *et al.* (1962) and Δ the epicentral distance in degrees. Data have been taken for each determination from 10 to 25 stations of the WWSSN System. The values found for m_b are in all cases larger than those of m_{CGS}, the magnitudes determined by the USCGS. The procedure used here for the determination of body waves magnitudes is somewhat different than the most usual one in which the largest amplitude in the P wave group is measured in short period records. However, in the absence of a universally accepted method of determining magnitudes, we estimate that the long period amplitudes, as measured here, provide uniform values of magnitude, lessening the effects of the local structure of the crust under the station.

To improve the determination of magnitude, the amplitudes have been corrected for the azimuthal effect of the source mechanism. For the P wave, this correction is

done in a somewhat different and simpler way as that used by Chandra (1970). Here, since the amplitude of the first cycle is used, we take directly the amplitude radiation pattern for the P wave due to a double-couple point source (Stauder 1960)

$$u_a = \frac{2}{4\pi\rho}\frac{xy}{a^3 R^3} K'\left(t - \frac{R}{a}\right)$$

where

$$x = \bar{x}\alpha_x + \bar{y}\beta_x + \bar{z}\gamma_x$$
$$y = \bar{x}\alpha_y + \bar{y}\beta_y + \bar{z}\gamma_y$$

α_x, β_x, γ_x and α_y, β_y, γ_y are the direction cosines of the X and Y axes of the focal mechanism, $\bar{x}$, $\bar{y}$, $\bar{z}$ are the co-ordinates of the station reduced to the focal sphere (positive: north, east and down). The ground motion amplitude of the P wave is corrected dividing by the azimuthal factor $2xy$ and multiplying by 0·424, the average value of this factor over a sphere. The corrected amplitude is, then, given by

$$A' = \frac{0{\cdot}424A}{2xy}.$$

This procedure does not give good results when the value of $2xy$ is very small, that is, for stations corresponding to rays leaving the source very near one of the nodal planes.

For surface waves, the correction of amplitude for the azimuthal effect of a vertical strike-slip fault is given by

$$A' = \frac{0{\cdot}638A}{\sin 2\theta}, \tag{4}$$

Table 4

Value of magnitude

	m USCGS	M PAS	M BRK	m_b uncorrected	M_s uncorrected	m_b corrected	M_s corrected
ALEUT	6·0	6¾–7	6–6½	6·53±0·40	7·03±0·17	7·07±0·20	7·16±0·18
NORAT1	6·1	6·9	6¾–7	6·63±0·24	6·80±0·18	6·83±0·11	6·65±0·18
NORAT2	5·9	6¼–6½	5½–5	6·45±0·28	6·56±0·25	6·61±0·16	6·48±0·22
AZORES	5·4	—	—	5·75±0·28	5·31±0·16	5·77±0·30	5·35±0·32

where θ is the azimuth from the strike of the fault, and the constant 0·638 the average value of $\sin 2\theta$ over a circle. Corrected and uncorrected magnitudes are given in Table 4. The large difference between m_b and M_s for ALEUT disappears after the correction is applied. The magnitude of ALEUT is greater than that of NORAT1, in agreement with the values found for the seismic moments. The low magnitudes reported for ALEUT can be, then, attributed to an effect of the particular orientation of its focal mechanism. Fig. 1 shows m_b versus M_s together with the known Richter's relation between these two values. The corrected magnitudes fit very closely the relation, except in the case of NORAT1 whose corrected surface wave magnitude is somewhat low.

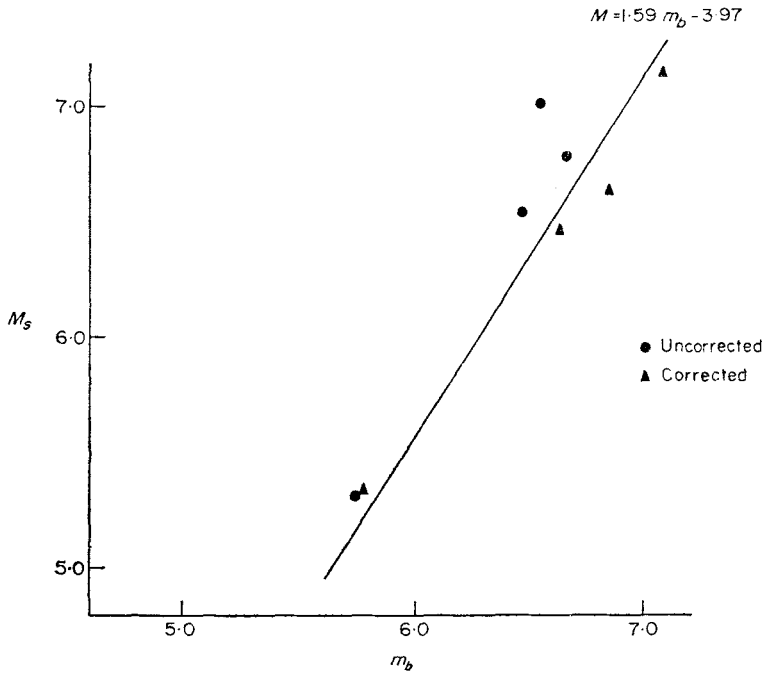

FIG. 1. Body wave magnitude versus surface wave magnitude.

Length of fault and velocity of rupture

Ben-Menahem (1961) has developed the theoretical expressions for the far field displacements of Rayleigh waves radiating from a propagating fault of finite dimensions. The model of the fault is a surface of length b and width d. The fracture is represented by a line of point sources moving in one direction with a finite velocity v and radiating energy as it propagates.

For a vertical strike slip fault, the line of sources occupies the vertical extent of the fault d and propagates along b with velocity v. The displacement of the vertical component of the Rayleigh wave for a propagating couple is given by

$$U_z^R = \frac{\sin 2\theta}{\sqrt{r}} g_z(\omega) \sqrt{(k_\beta)} \left\{\frac{\sin X_R}{X_R}\right\} \exp\left[i\left(\phi_R + \frac{3\pi}{4}\right)\right] \tag{5}$$

where

$$X_R = \frac{\pi b}{\lambda}\left(\frac{c_R}{v} - \cos\theta\right). \tag{6}$$

$$\phi_R = \omega\left(t - \frac{r}{c_R}\right) - X_R. \tag{7}$$

C_R is the Rayleigh wave phase velocity, r the epicentral distance, θ the azimuth to the station measured counterclockwise from the strike of the fault, and k_β the wave number of shear waves. $g_z(\omega)$ is a function which depends on the source time function, the width of the fault, depth and frequency. The effect of the finite dimensions is included in the factor X_R and the phase ϕ_R. To isolate this effect, Ben-Menahem has defined the 'directivity function' as the ratio of the spectral amplitudes

of surface waves corresponding to rays leaving the source in opposite directions.

$$D = \frac{|U_z^R(\theta)|}{|U_z^R(\theta+\pi)|} = \frac{\left|\sin\left[\frac{\pi bf}{c_R}\left(\frac{c_R}{v}-\cos\theta\right)\right]\left(\frac{c_R}{v}+\cos\theta\right)\right|}{\left|\sin\left[\frac{\pi bf}{c_R}\left(\frac{c_R}{v}+\cos\theta\right)\right]\left(\frac{c_R}{v}-\cos\theta\right)\right|}. \tag{8}$$

Another way of isolating the effect of the finiteness of the source is through the differential phase, but this method will not be treated here, and only the amplitude part of the spectra will be used. Since the only factors in equation (5) which depend on θ are X_R and $\sin 2\theta$, the expression for the directivity function can be generalized to include the amplitude ratios of the displacements of any two rays leaving the source with an arbitrary angle α between them. Thus

$$D_\alpha = \frac{|U_z^R(\theta)|}{|U_z^R(\theta+\alpha)|} = \frac{\left|\sin\left[\frac{\pi bf}{c_R}\left(\frac{c_R}{v}-\cos\theta\right)\right]\left(\frac{c_R}{v}-\cos(\theta+\alpha)\right)\sin 2\theta\right|}{\left|\sin\left[\frac{\pi bf}{c_R}\left(\frac{c_R}{v}-\cos(\theta+\alpha)\right)\right]\left(\frac{c_R}{v}-\cos\theta\right)\sin 2(\theta+\alpha)\right|}. \tag{9}$$

For the special case when $\alpha = 90$ degrees, the expression for D_α takes the form

$$D_{90} = \frac{\left|\sin\left[\frac{\pi bf}{c_R}\left(\frac{c_R}{v}-\cos\theta\right)\right]\left(\frac{c_R}{v}+\sin\theta\right)\right|}{\left|\sin\left[\frac{\pi bf}{c_R}\left(\frac{c_R}{v}+\sin\theta\right)\right]\left(\frac{c_R}{v}-\cos\theta\right)\right|}. \tag{10}$$

For a strike-slip fault with an arbitrary dip angle, the expression for the vertical component of the displacement of the Rayleigh waves includes, besides the factor $\sin X_R/X_R$ factors of the form $\sin \Lambda_1^R/\Lambda_1^R$ and $\sin \Lambda_2^R/\Lambda_2^R$, where

$$\Lambda_1^R = \frac{\omega d}{2c_R}\left(\sin\theta\cos\delta + i\frac{\sqrt{(\gamma^2-1)}}{\gamma}\sin\delta\right), \tag{11}$$

$$\Lambda_2^R = \frac{\omega d}{2c_R}\left(\sin\theta\cos\delta + i\frac{\sqrt{(\gamma^2-\frac{1}{3})}}{\gamma}\sin\delta\right). \tag{12}$$

These factors cancel out when taking the ratio D of the amplitudes for rays separated by 180 degrees. Therefore, as was already pointed out by Ben-Menahem, the directivity function D is independent of dip for a strike-slip fault. For the generalized D_α this is not true. However, since d, the width of the fault, can be safely assumed for strike-slip motion to be smaller than the length b, its influence will also be small, and equation (9) for D_α will give, even in this case, good estimates of the values of b and v.

For a vertical dip-slip fault, the model representing the fault is a line of point sources which move downward with velocity v. It should be noted that in the horizontal dimension all point sources move downward simultaneously; that is, there is no propagation of the fracture in the b direction. For $\alpha = 180$ the directivity function

is equal to unity for all values of θ. For other values of α it has the form

$$D_\alpha = \frac{\left|\sin\left(\frac{\omega b}{2c_R}\cos\theta\right)\cos(\theta+\alpha)\right|}{\left|\sin\left(\frac{\omega b}{2c_R}\cos(\theta+\alpha)\right)\cos\theta\right|}. \tag{13}$$

This equation gives only an estimate of b, the length of the vertical fault. The parameters d and v, which are involved in the downward propagation of the fault, appear in the expression for the displacement of Rayleigh waves in factors which do not depend on θ and cancel out when taking the ratios.

New tectonic theories and the observed nodal plane solutions of P for many earthquakes have pointed to a frequent occurrence of very low angle thrust faults. These can be approximated by faulting on a horizontal plane. The expression for the directivity function of such a model can be derived from that of the strike-slip case by making the dip angle equal to zero. Then we will have from equation (11) and (12)

$$\Lambda_1{}^R = \Lambda_2{}^R = \frac{\omega d}{2c_R}\sin\theta. \tag{14}$$

The general form for D_α is

$$D_\alpha = D_\alpha' \frac{\left|\sin\left(\frac{\omega d}{2c_R}\sin\theta\right)\sin(\theta+\alpha)\right|}{\left|\sin\left(\frac{\omega d}{2c_R}\sin(\theta+\alpha)\right)\sin\theta\right|}, \tag{15}$$

where D_α' is the expression for the vertical strike-slip case. For the case when $\alpha = 180$ the two expressions are obviously the same.

For dip-slip motion with an arbitrary dip angle, the displacement fields for the Rayleigh wave have a more complicated form, and the ratios of the amplitudes do not have the simple forms we have found in the other cases.

The models for propagating faults presented up to this point are those considered by Ben-Menahem (1961). In all of them the fracture propagates with a finite velocity only in one direction which is the same as that of the forces of the point sources, while in the direction perpendicular to it all points move simultaneously. In other words, the fault starts as a line source that propagates in one direction. This assumption is very reasonable but may not be always the case. A fracture can start at a point and propagate progressively with a finite velocity in two perpendicular directions. If this is so, it is easy to show that if b is the horizontal dimension of the fracture and v the velocity of fracture in that direction for any orientation of the forces, the directivity will provide us with an estimate of the horizontal dimension of the fault, independent of the orientation of the forces (Press 1964).

Determination of b and v from the generalized directivity

The directivity function D as defined originally (equation (8)) was used with R or G waves of consecutive order recorded at the same station. This procedure minimizes the sources of error but reduces also the use of the method to earthquakes

sufficiently large to generate return surface waves or waves which circle the Earth at least once. For smaller earthquakes, in theory, nothing prevents using direct Rayleigh or Love waves recorded at different stations distributed at arbitrary but differing azimuths about the epicentre. The advantage of applying in this case the more generalized expression for the directivity, D_α (equation (9)), is that stations can be selected at which the Rayleigh waves are well recorded without the constraint of being 180° apart in azimuth. Allowance must be made, of course, for differences in epicentral distance, path of propagation, etc. This procedure makes it possible to apply the method to earthquakes smaller than $M = 7$.

The shape of the curve for D_α as a function of frequency for fixed values of b and v and known phase velocity dispersion has a series of maxima and minima. Minima occur at zeros of the numerator, that is, at values of the argument of the sine function

$$\frac{\pi bf}{c_R}\left(\frac{c_R}{v}-\cos\theta\right)=n\pi, \qquad n=1, 2, 3, \ldots . \tag{16}$$

Maxima occur at zeros of the denominator or for

$$\frac{\pi bf}{c_R}\left(\frac{c_R}{v}-\cos(\theta+\alpha)\right)=n\pi, \qquad n=1, 2, 3, \ldots . \tag{17}$$

The values of the frequency at which either maxima or minima occur can be used to determine the fault length. The first maximum and minimum, that is, the maximum and minimum corresponding to the lowest frequencies, are especially suitable for this. Putting $n = 1$ in equations (16) and (17) and solving for b, we obtain

$$b=\frac{c_R}{f_{\max}\left(\frac{c_R}{v}-\cos(\theta+\alpha)\right)}=\frac{c_R}{f_{\min}\left(\frac{c_R}{v}-\cos\theta\right)}. \tag{18}$$

Using many ratios of observed spectral amplitudes from different pairs of stations, an estimate of the length b can be obtained as the mean of the values from each pair. In so doing, it is necessary to assume a value of v, the velocity of rupture. In fact, when using only the amplitude portion of the spectra there is no independent way of determining the fracture velocity. However, if many ratios are used for the calculation of b, we can assume different values of v and from these select that v which gives the least standard error for the mean value of b. In this manner, a simultaneous estimate of both b and v can be obtained. The accuracy and reliability of the results will, in fact, increase with the number of pairs of stations used. It is here where one can see the advantage of using the generalized form of the directivity function, D_α, since it permits more combinations of pairs of stations.

As a function of θ, the shape of the curve changes in a different way for different values of α. For $\alpha = 180$ it is symmetrical with respect to $\theta = 0°$ and $\theta = 90°$ so that

$$D_{180}(\theta)=D_{180}(-\theta),$$

$$D_{180}(90+\theta)=\frac{1}{D_{180}(90-\theta)}.$$

D_{180} has a maximum in the first and fourth quadrant and a minimum in the second and third. For $\theta = 90°$, $D_{180} = 1$ for all values of frequency. For $\alpha = 90$ the directivity function is unity for $\theta = 135°$ and at $\theta = 45°$, $D_{90} = D_{180}$.

The pattern of the occurrence of the first extreme value as a maximum or a minimum at different azimuths serves to identify the true fault plane from the two given nodal planes, as well as the direction of rupture propagation. Fig. 2 illustrates how this is done. The observed directivity for $\alpha = 180$ is given by the ratios of the spectral amplitudes at stations S_1, S_2, S_3 and S_4 taken in the following order: $D_{13} = S_1/S_3$, and $D_{24} = S_2/S_4$. The occurrence of the first extreme value of the directivity as a minimum or a maximum in the two ratios D_{13} and D_{24} for each of the four possible directions of rupture is indicated in the same figure. Consequently, if the orientation of the two planes is known, with only two ratios of amplitudes from stations in the four quadrants, the true fault plane and the direction of fracture are uniquely determined.

The lowest frequency at which the first maximum or minimum of D_α appears is controlled mainly by the value of b. For large faults the first extreme value corresponds to low frequencies. The influence of v, the rupture velocity, is to shift the first maximum or minimum toward higher frequencies and to increase the frequency interval between two extreme values, as v takes larger values. An example of the effect of b and v on the theoretical values of D_α can be seen in Figs 3 and 4.

The fifth variable appearing in the expression for D_α is c_R, the Rayleigh wave phase velocity. Since it is not always possible to know with accuracy the phase velocity

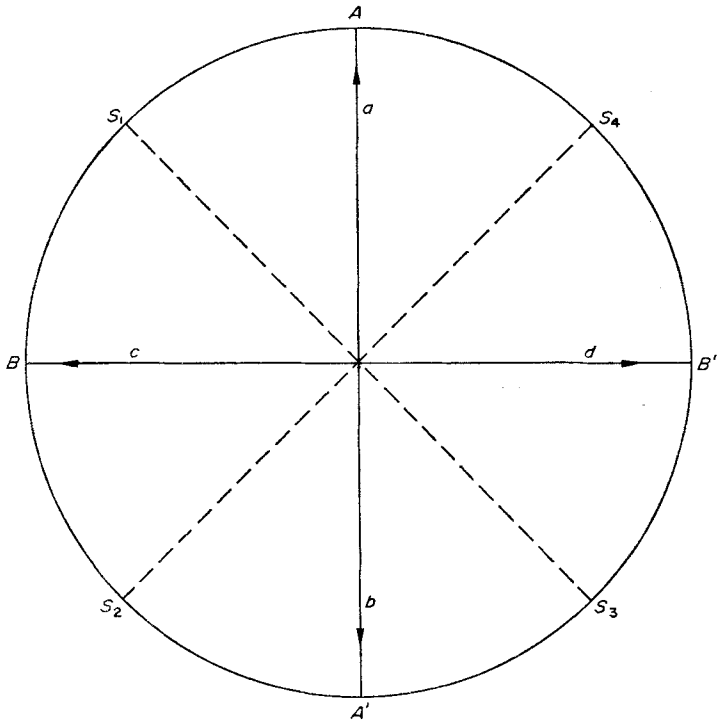

Rupture	D_{13}	D_{24}
AA' a	max	min
AA' b	min	max
BB' c	max	max
BB' d	min	min

FIG. 2. Maxima and minima of the directivity and its relation to the direction of rupture propagation.

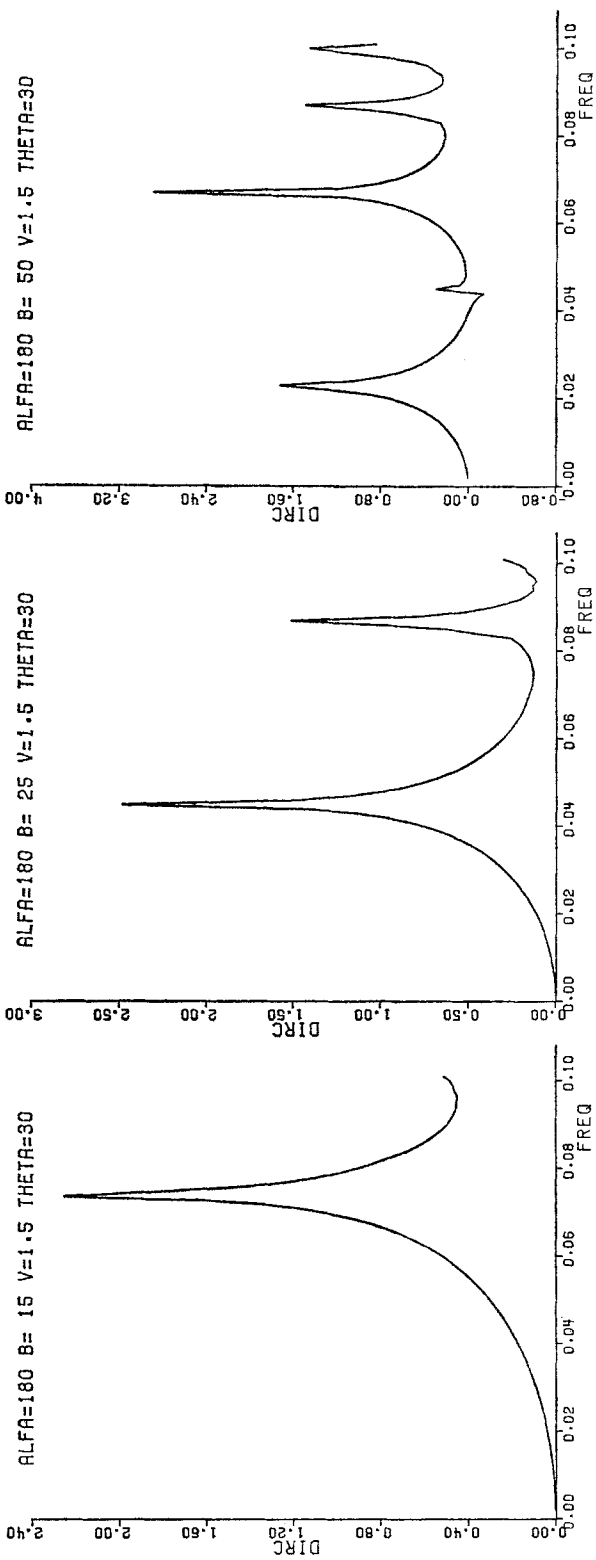

FIG. 3. Directivity function for different values of the fault length b.

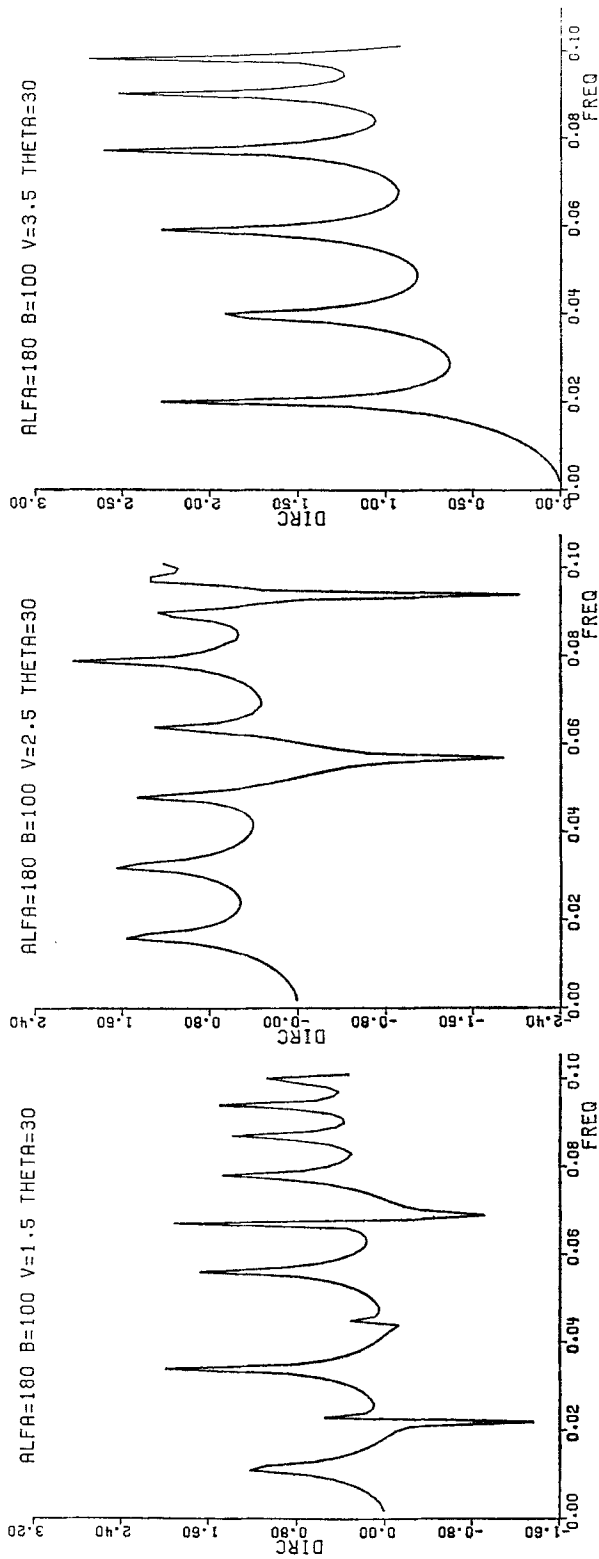

FIG. 4. Directivity function for different values of the velocity of fracture v.

dispersion curve for all the paths involved, c_R will introduce errors in the determination of b. For low frequencies, the uncertainties in the phase velocity are small, but for higher frequencies, the influence of the local condition of the crust is very important, and phase velocity curves for all paths are not available. However, this influences very little the determination of b. For values of b of the order of 50 km a change in the value of c_R of 0·6 km s^{-1} affects the determination of b by only 1·5 km.

Application

Values of the fault length and rupture velocity have been determined for the four selected earthquakes. A number of stations from the WWSSN were selected which have clear, undisturbed records of the direct Rayleigh waves in the long period vertical component instrument. The Rayleigh waves at these stations were digitized and a Fourier analysis made of the digitized data. In this process, care must be taken to select a suitable time window, for it is important to exclude from the analysis any interference from later arrivals, lateral refractions, etc., which may introduce holes in the spectra totally unrelated to the fault dimensions. Some examples of the amplitude spectra obtained are given in Fig. 5. The spectra are fairly flat in the long period range. Since the directivity function is normalized, the amplitudes in the spectral ratios were reduced to a common distance by reducing the amplitudes of the second station to the distance of the first through equation

$$A_2{}^1 = A_2 \left(\frac{\sin \Delta_1}{\sin \Delta_2}\right)^{\frac{1}{2}} \exp\left[-(\Delta_1 - \Delta_2)\gamma\right]. \tag{19}$$

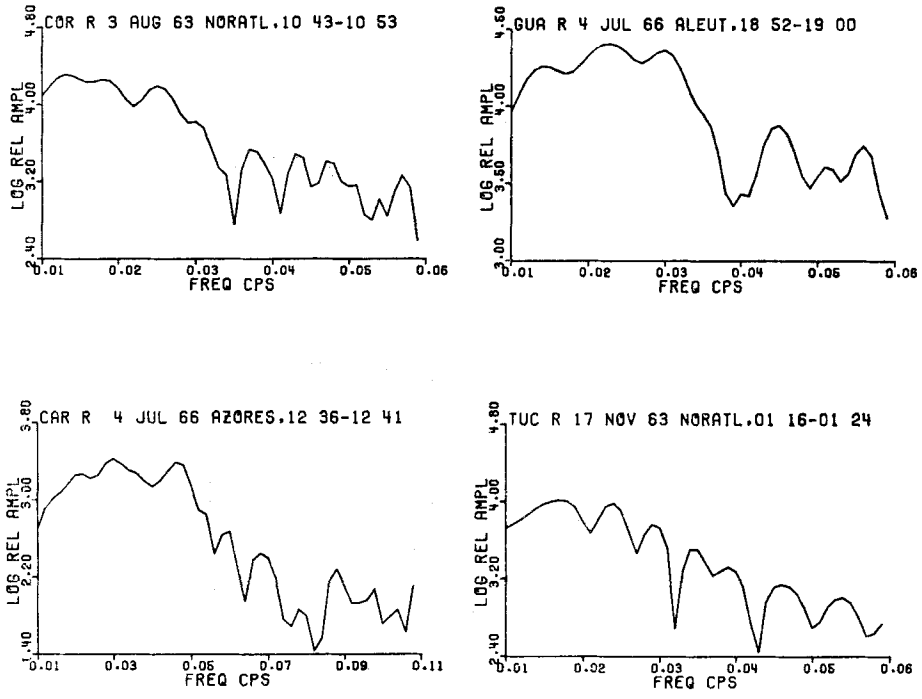

FIG. 5. Examples of the amplitude density spectra.

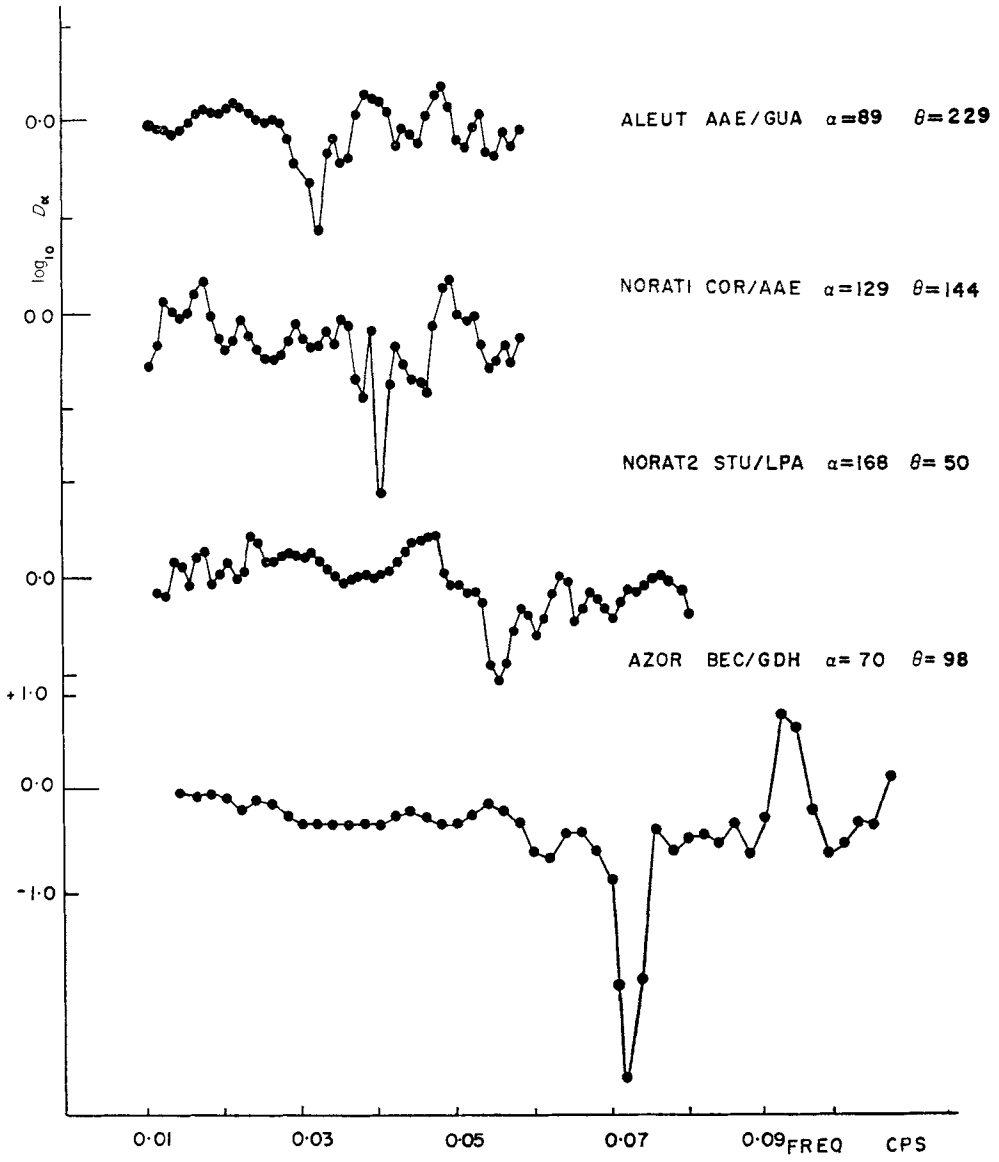

FIG. 6. Observed values of the directivity for each of the four earthquakes.

A_2 is the spectral amplitude at the second station, Δ_1 and Δ_2 the epicentral distances of the first and second stations, and γ the attenuation coefficient. Examples of the observed values of the directivity function for the four earthquakes are shown in Fig. 6. The first observed minimum moves toward higher frequencies as the magnitude of the event decreases.

For ALEUT, Rayleigh waves from nine stations were used. The situation of the stations with respect to the strikes of the two nodal planes AA' and BB' is given in Fig. 7. Of these two planes, plane AA' has been selected as the fault plane with the fracture propagating toward the south. The selection is done on the basis of the observed maxima and minima of the directivity function at different azimuths, as explained above. This direction gives minima for D_{180} with the first station in any

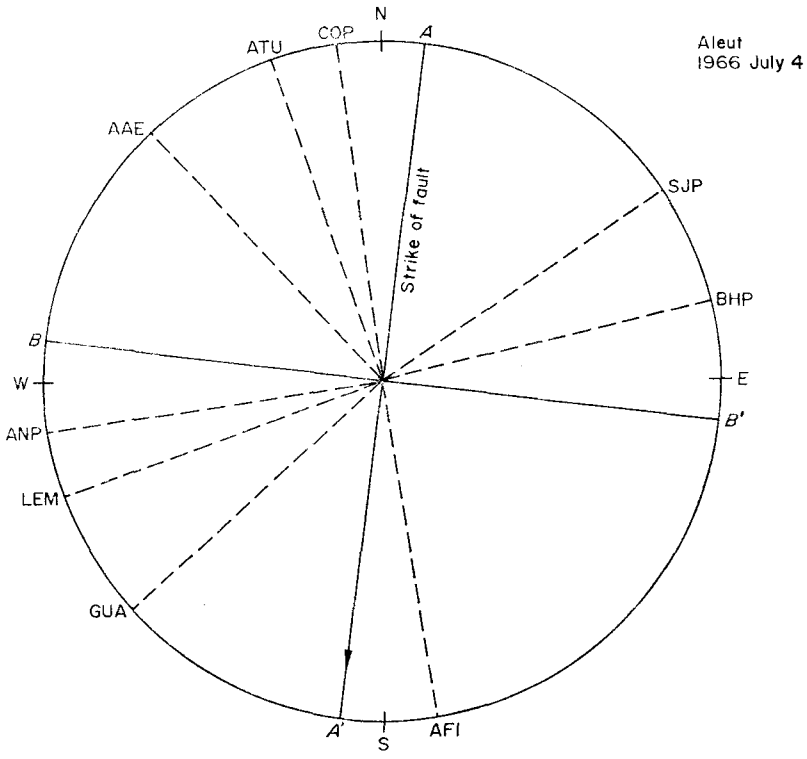

FIG. 7. Azimuthal location of the stations used for ALEUT with respect to the strike of the two nodal planes. The arrow on the strike of the fault plane represents the direction of rupture propagation.

of the two northern quadrants, and maxima when the first station is in any of the southern ones.

The pairs of the stations used to find the ratios of the spectral amplitudes, together with the frequencies of the first maximum or minimum, and the derived values for b are given in Table 5. The least scattering in these values was obtained using $v = 1{\cdot}5\,\mathrm{km\,s^{-1}}$; for comparison, those corresponding to $v = 3{\cdot}0\,\mathrm{km\,s^{-1}}$ are also given in the same table. Their means are respectively

$$v = 1{\cdot}5\,\mathrm{km\,s^{-1}} \qquad b = 35 \mp 3{\cdot}4\,\mathrm{km}$$

$$v = 3{\cdot}0\,\mathrm{km\,s^{-1}} \qquad b = 67 \mp 17{\cdot}6\,\mathrm{km}.$$

The frequencies at which the first maximum and minimum of the directivity occur are shown in Fig. 8 as a function of θ. The theoretical curves correspond to the derived values of b and v and for $\alpha = 180°$ and $\alpha = 90°$. The observations fall relatively close to the theoretical curve and are in all cases consistent with the determined direction of fracture. Three examples of the fit of the theoretical to the observed values of the directivity for the ratios ANP/BHP, ANP/AFI, and ATU/AFI are given in Fig. 9. Not only the position of the extreme value, but the general shape of the curve agrees with the theoretical. The occurrence of the first maximum and minimum close together for ANP/BHP and the minimum at higher frequencies for ANP/AFI are in agreement with what is expected at the given values of the azimuth.

Table 5

Frequencies of minima and maxima of D_α for ALEUT

Stations	θ	α	f_{min}	f_{max}	b (km) ($v = 1{\cdot}5$)	b (km) ($v = 3{\cdot}0$)
COP/AFI	195	181	0·038		29·3	44·8
ATU/AFI	206	170	0·035		31·8	50·2
ANP/BHP	286	186	0·043	0·032	39·0 42·4	89·1 77·0
LEM/BHP	297	175	0·046	0·032	39·5 39·9	101·6 69·0
SJP/AAE	122	90		0·032	35·3	56·2
ATU/ANP	206	79	0·035		32·2	51·1
ATU/LEM	206	90	0·035		32·2	51·1
AAE/GUA	229	89	0·032		37·4	61·7
ANP/AFI	286	91	0·043		39·0	89·1
AFI/BHP	16	95		0·038	35·7	64·8

For AZORES, Rayleigh wave data from eight stations were used. The location of the stations with respect to the two nodal planes defined from the body waves is given in Fig. 10. The fault plane which gives the best fit of the observations of the directivity with that of the theoretical model is AA' and the direction of propagation of fracture toward north. The plane selected corresponds to that with the greater strike-slip component of motion. The frequencies at which the first maximum or minimum occur for the six amplitude ratios used in this earthquake, together with the resulting values for b for two different fracture velocities are given in Table 6. The extreme values appear at higher frequencies than those for ALEUT, as expected for a smaller earthquake. Mean values of b for the assumed rupture velocities are

$$v = 1{\cdot}5\ \mathrm{km\,s^{-1}} \qquad b = 18 \pm 1{\cdot}8\ \mathrm{km}$$

$$v = 3{\cdot}0\ \mathrm{km\,s^{-1}} \qquad b = 31{\cdot}5 \pm 4{\cdot}3\ \mathrm{km}.$$

Here again a low rupture velocity gives the best fit to the observed values of directivity. Some examples of the observed and theoretical directivity curves are given in Fig. 11.

Table 6

Frequencies of minima and maxima of $D\alpha$ for AZORES

Stations	θ	α	f_{min}	f_{max}	b $v = 1{\cdot}5$	b $v = 3{\cdot}0$
CAR/STU	130	191	0·082		14·2	24·3
TRI/STU	126	186	0·064		18·6	32·0
TRI/IST	126	172	0·064		18·6	32·0
GDH/BEC	25	70		0·072	20·0	39·0
STU/GDH	313	71	0·064		18·0	30·5
GDH/TRI	25	103		0·064	18·4	31·5

For NORAT1 and NORAT2, a smaller number of stations was available with well-recorded Rayleigh waves. In the analysis only four stations were used for the first and five for the second. The determination of the length of the faults is, therefore, less accurate than for the two other earthquakes. The selected plane of faulting

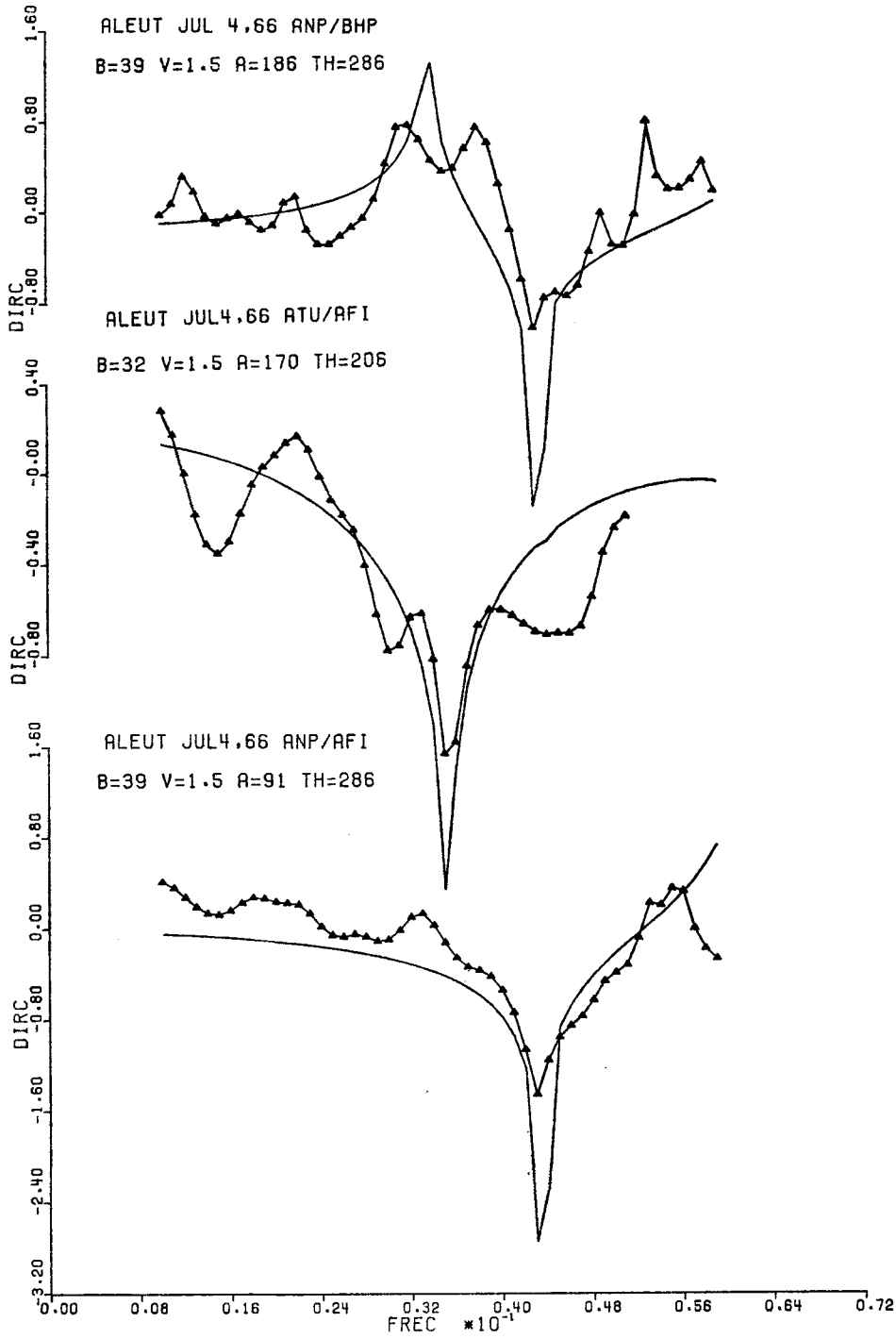

FIG. 8. Observed and theoretical directivity for ALEUT.

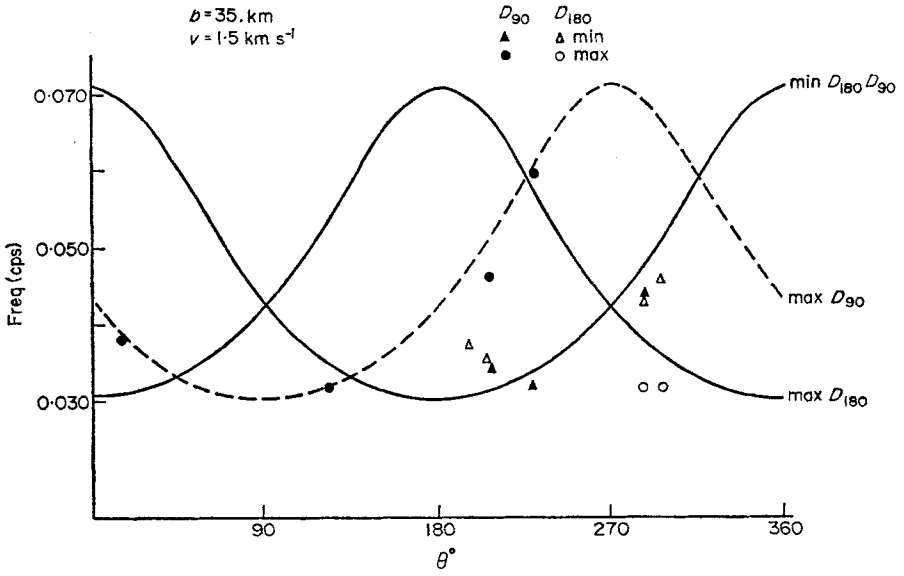

FIG. 9. Observed and theoretical values of the frequencies at which the first minimum and maximum of the directivity function $D\alpha$, as a function of the azimuth angle θ.

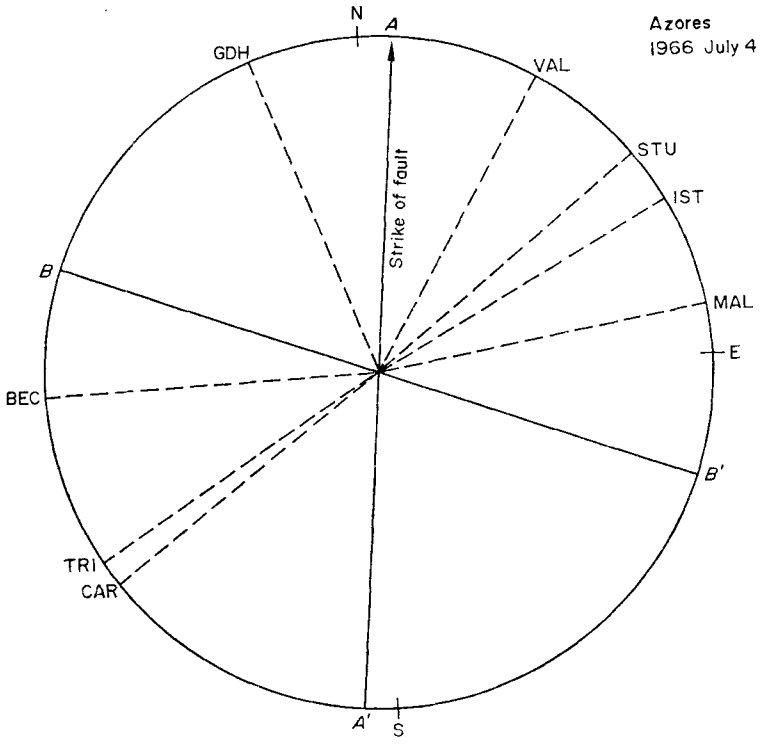

FIG. 10. Azimuthal location of the stations used for AZORES with respect to the strikes of the two nodal planes. The arrow on the strike of the fault plane represents the direction of rupture propagation.

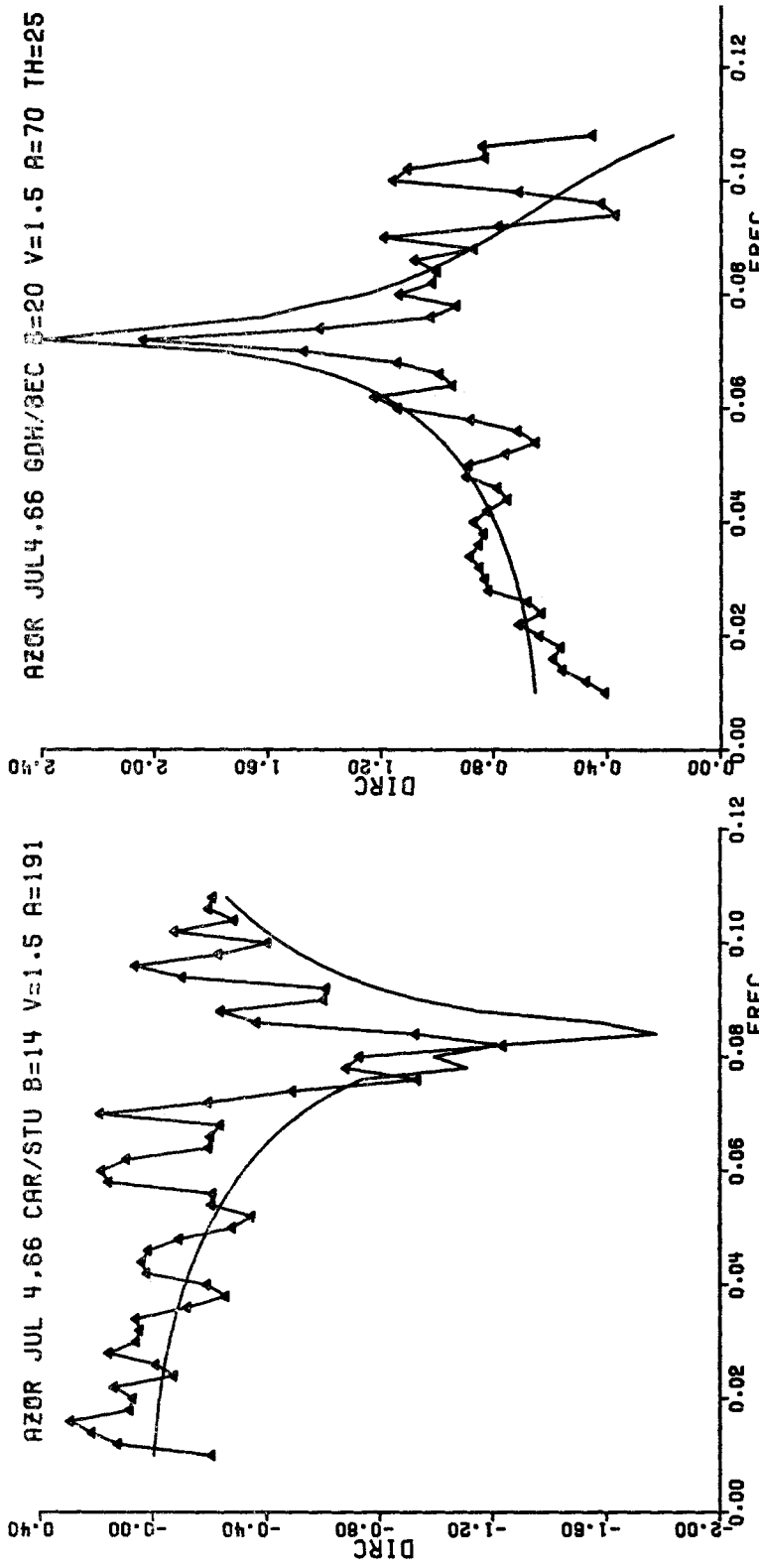

FIG. 11. Observed and theoretical directivity for AZORES.

in both cases is the one striking EW, with the direction of propagation toward the east. This result agrees with the interpretation of these two earthquakes as motion on a transform fault in the mid-Atlantic Ridge. Assuming a value of $v = 1{\cdot}5\,\mathrm{km\,s^{-1}}$, the value of the length of the faults are

$$\text{NORAT1} \qquad b = 32 \pm 2{\cdot}0\,\mathrm{km}$$

$$\text{NORAT2} \qquad b = 27 \pm 6{\cdot}7\,\mathrm{km}.$$

The values obtained for the lengths of the fault and rupture velocities for these four earthquakes point to a time duration of the rupture process of the order of 10 to 20 s.

Seismic moment

For the source of an earthquake considered as a sudden dislocation on a plane surface, the seismic moment has been defined as the product of the area of the fault A by the rigidity μ and the average dislocation or displacement over the fault surface $\bar{w}$ (Wyss & Brune 1968)

$$M_0 = \mu A \bar{w}. \tag{20}$$

If the point source approximation for the focus of an earthquake is valid, the moment of the assumed couple of forces acting at a point will also represent the total seismic moment. If this assumption is correct, we can derive M_0 from the theoretical expressions for the far field displacement for point sources. Following the work of Aki (1966) and the theoretical results of Ben-Menahem & Harkrider (1964), an expression can be derived for the seismic moment in terms of the spectral amplitudes of the Rayleigh waves. Assuming a step function for the source time function, the value of the moment is given by

$$M_0 = \frac{|\, U_z^R(w)\,|\,(2\pi r)^{\frac{1}{2}} c_R\, e^{\gamma r}}{N_{rz}\,|\,X(\theta)\,|}, \tag{21}$$

where $U_z^R(\omega)$ is the spectral amplitude, r the distance, γ the attenuation coefficient, c_R the phase velocity, N_{rz} the Rayleigh wave singlet transfer function, and $\chi(\theta)$ the radiation pattern function as defined by Ben-Menahem & Harkrider. For the earthquakes studied here, the moment has been determined at two values of the period, 100 and 50 s. These periods correspond to the first part of the observed spectra. For earthquakes of these sizes their Rayleigh wave amplitudes can be reasonably approximated by those of a point source.

The values for the seismic moment are given in Table 7. In the third column of the table are the means of all data from 100 and 50 s taken together. In a recent

Table 7

Seismic moment in dyne-cm

	M_0 100 s	M_0 50 s	$\bar{M}_0$
ALEUT	$1{\cdot}4 \pm 0{\cdot}37 \times 10^{26}$	$3{\cdot}1 \pm 1{\cdot}19 \times 10^{26}$	$2{\cdot}26 \pm 1{\cdot}23 \times 10^{26}$
NORAT1	$1{\cdot}2 \pm 0{\cdot}97 \times 10^{26}$	$1{\cdot}4 \pm 0{\cdot}74 \times 10^{26}$	$1{\cdot}22 \pm 0{\cdot}76 \times 10^{26}$
NORAT2	$2{\cdot}2 \pm 0{\cdot}49 \times 10^{25}$	$5{\cdot}5 \pm 0{\cdot}76 \times 10^{25}$	$3{\cdot}83 \pm 1{\cdot}79 \times 10^{25}$
AZORES	$2{\cdot}4 \pm 0{\cdot}93 \times 10^{24}$	$1{\cdot}5 \pm 0{\cdot}44 \times 10^{24}$	$1{\cdot}96 \pm 0{\cdot}85 \times 10^{24}$

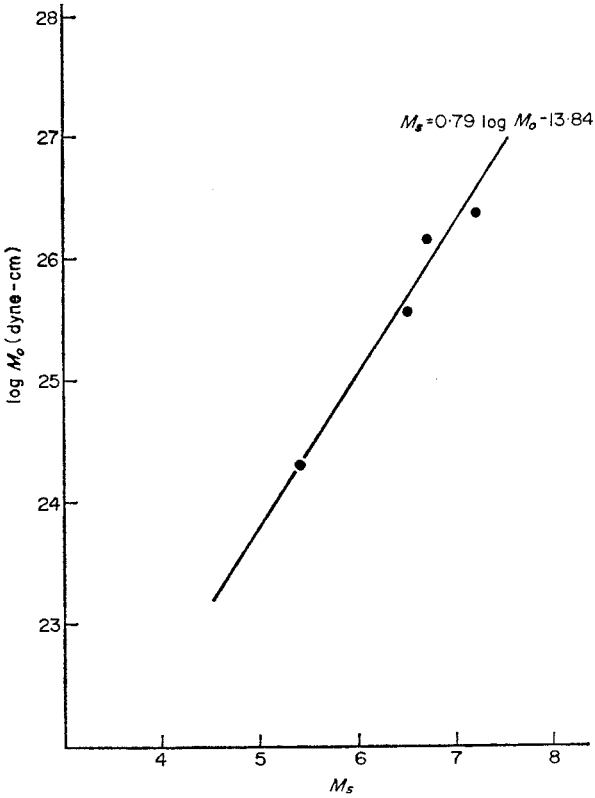

FIG. 12. Seismic moment versus surface wave magnitude.

study of the relations between the various fault parameters, Chinnery (1969) suggests a linear relation between the magnitude and what he calls the ' geometrical moment ', defined as the product of the fault area by the dislocation. This relation is given by

$$M = (0{\cdot}79 \mp 0{\cdot}06) \log_{10} LDW - (4{\cdot}74 \mp 0{\cdot}86),$$

where L is the fault length, D the width and W the dislocation. Taking the definition of M_0 from equation (20) and assuming a value of $\mu = 3{\cdot}3 \times 10^{11}$ dyne cm^{-2}, the above relation can be expressed in terms of M_s and M_0 in the form

$$M_s = 0{\cdot}79 \log_{10} M_0 - 13{\cdot}84. \tag{22}$$

This relation fits very well to our data as can be seen in Fig. 12. The values of M_0 determined here referred to the moment of the couple of forces assumed as the point source model of earthquakes, while Chinery's relation is based on data of observed or derived values of the length and dislocation on faults. The agreement shown in Fig. 12 shows the equivalence of the two definitions of the seismic moment.

Seismic energy, stress drop and average dislocation

Up to this point, we have been able to determine from the direct analysis of seismic waves the magnitude, fault length, rupture velocity, and the total seismic moment of an earthquake. From these parameters others can be derived that are useful in order to describe the nature of a seismic source. First, from the values of the magnitude the seismic energy E_s can be determined through the relations (Richter 1958)

$$\log E_s = 5{\cdot}8 + 2{\cdot}4\, m_b, \tag{23}$$

$$\log E_s = 11{\cdot}8 + 1{\cdot}5\, M_s. \tag{24}$$

The seismic energy E_s is related to the total energy released during an earthquake through the seismic efficiency factor η

$$E_s = \eta E. \tag{25}$$

If it is assumed that the energy is released in an earthquake by slipping on a fault surface, the total energy can be written as the product of the average shear stress $\bar{\sigma}$ by the area of the fault A and the average dislocation or displacement on the fault $\bar{w}$ (Brune 1968)

$$E = \bar{\sigma} A \bar{w}. \tag{26}$$

The average dislocation $\bar{w}$ can be derived from the value of the seismic moment in equation (20). Assuming a rectangular fault surface of length b and width d, we obtain

$$\bar{w} = \frac{M_0}{\mu b d}. \tag{27}$$

Substituting this value in equation (26) and using equation (25) we obtain for the product of the average stress $\bar{\sigma}$ and the seismic efficiency factor η the expression

$$\eta \bar{\sigma} = \frac{\mu E_s}{M_0}. \tag{28}$$

The difference in shear stress acting on a fault surface before and after the occurrence of an earthquake is generally referred to as the stress drop σ. This is related to the maximum dislocation w_m through the equation (Brune & Allen 1967)

$$\sigma = \xi \frac{w_m \mu}{d}. \tag{29}$$

where ξ is a constant ranging from 1/2 to $2\pi/3$, depending on the fault geometry. For a vertical strike-slip fault $\xi = \frac{1}{2}$. The maximum displacement on the fault is usually taken as $\frac{4}{3}$, the value of the average displacement $\bar{w}$. Taking this relation and substituting the resulting value for $\bar{w}$ of equation (27) into equation (28), we obtain for the stress drop in a vertical strike-slip fault

$$\sigma = \frac{4}{6} \frac{M_0}{b d^2}. \tag{30}$$

Thus, the stress drop is independent of the assumed value of the rigidity but depends strongly on the value of the fault width d.

The expressions for the average dislocation and the stress drop (equations (29) and (30)) both include the value of the fault width. The directivity function, as we have seen, gives us only an estimate of the length, but no information about the width. For earthquakes with well-recorded aftershocks, an estimate of d is possible from the aftershock area. The method described by Chinnery (1961) requires a detailed knowledge of the movements of the ground at the time of the earthquake, which in very few cases is possible. For vertical strike-slip faults, if surface breaking is observed, the depth of the focus may give an estimate of d. However, for most earthquakes not even this is possible. The width of the fault remains, then, very much a matter of assumption. For vertical strike-slip faults the width can be safely assumed to be less than the length; in our calculations we have assumed it to be of the order of $\frac{1}{3}$ the value of the length.

Table 8

Source parameters

	E_s 10^{21} erg	M_0 10^{25} dyne-cm	b km	d km	$\bar{w}$ cm	σ bars	$\eta\bar{\sigma}$ 10^7 dyne cm^{-2}
ALEUT	46·6	22·6	35	12	163	30	5·06
NORAT1	10·0	12·2	32	11	105	21	2·71
NORAT2	4·41	3·83	27	9	47·7	11·7	3·80
AZORES	0·0556	0·196	18	6	5·49	2·1	1·12

For the four earthquakes under study, the values of these parameters are given in Table 8. The seismic energies are the averages of the values found from m_b and M_s using equations (23) and (24). The stress drops are relatively small. These are, as was already mentioned, strongly dependent on the assumed widths of the faults. The values of b and σ for ALEUT are very similar to those found for the same earthquake by Khattri & Stauder (1970) using the spectra of body waves ($b = 38$ km and $\sigma = 34$ bars). While the values of the stress drops decrease with decreasing magnitude, those of the average stress times the seismic efficiency factor remain fairly constant. If for these magnitudes the efficiency is considered constant, this indicates that the initial stress is independent of magnitude. Taking the efficiency to be close to unity, the order of magnitude of the average stress is 10^7 dyne cm^{-2}. This order of magnitude was given by Chinnery (1964) for the strength of the Earth's crust under horizontal shear stress.

The relation between the stress drop and the average stress depends on the mechanism of stress release. If, at the time of faulting, all the accumulated stress is released, then the two values must be of the same order. For AZORES the value of σ is one order of magnitude smaller than $\eta\bar{\sigma}$, while for the other three earthquakes they are in the same order. If we assume that the value of the efficiency factor η is close to unity and constant for all four earthquakes, the difference in our results can be interpreted as meaning that large earthquakes release all the acting stress, but smaller ones only a fraction. However, the same effect could be explained if the seismic efficiency decreases for smaller shocks, and all the accumulated stress is always released. More data from a wider range of magnitudes is needed to better understand these relations. Brune (1968) has determined values of $\eta\bar{\sigma}$ for earthquakes in California. For magnitudes greater than 6·0, his values are in the same order as ours, but for lower magnitudes they are two to three orders of magnitude smaller than ours.

Conclusions

A generalized directivity function has been defined that has proved useful in finding the horizontal dimensions of vertical strike slip faulting for earthquakes of magnitude below 7. For the magnitude range from 5·7 to 7·0, the dimension of the source varies from 18 to 35 km. Allowing for certain indeterminacy in the adjustment of the velocity of rupture, these values may be modified by small amounts. Since in all cases a velocity of rupture of 1·5 km s^{-1} was used, our values represent a low estimate of the length. For ALEUT and AZORES this low velocity of rupture gives the best fit to the directivity data.

Total seismic moments have been determined from the spectral amplitudes of Rayleigh waves and the theoretical expressions for the moment of point source models. For the four earthquakes, these values, in combination with those of length, give average dislocations between 4 and 164 cm and stress drops from 2 to 30 bars.

More data from different magnitude ranges and from different depths and focal mechanism orientation are needed for a better understanding of the relations between the source parameters.

Acknowledgments

This work was completed during the author's stay at the Department of Earth and Atmospheric Sciences of Saint Louis University. He wishes to express his thanks to Professors C. Kisslinger, W. Stauder and O. Nuttli for their suggestions and helpful discussions. He is also indebted to Patricia M. Righter for assistance in the calculation and in preparing the manuscript.

This work was supported by Project Vela Uniform under Contract F19628–70–C–0036 with the Geophysics Research Directorate, Air Force Cambridge Research Laboratories.

Department of Earth and Atmospheric Sciences,
School of Engineering and Earth Science,
Saint Louis University,
St Louis, Missouri.

References

Aki, K., 1966. Generation and propagation of G waves from the Niigata earthquake of June 16, 1964. 2. Estimation of earthquake moment, released energy, and stress-strain drop from the G wave spectrum, *Bull. Earthquake Res. Inst., Tokyo*, **44,** 73–88.

Banghar, A. R. & Sykes, L. R., 1969. Focal mechanism of earthquakes in the Indian Ocean and adjacent regions, *J. geophys. Res.*, **74,** 632–649.

Ben-Menahem, A., 1961. Radiation of seismic surface waves from a finite moving source, *Bull. seism. Soc. Am.*, **51,** 401–435.

Ben-Menahem, A. & Harkrider, D. G., 1964. Radiation pattern of seismic surface waves from buried dipolar point sources in a flat stratified earth, *J. geophys. Res.*, **69,** 2605–2619.

Brune, J. N., 1968. Seismic moment; seismicity and rate of slip along major fault zones, *J. geophys. Res.*, **73,** 777–784.

Brune, J. N. & Allen, C. R., 1967. A low-stress-drop, low-magnitude earthquake with surface faulting, the Imperial Valley California earthquake of March 4, 1966, *Bull. seism. Soc. Am.*, **57,** 501–514.

Chandra, U., 1970. Correction for focal mechanism in body wave magnitude determination, *J. geophys. Res.*, **75,** 3421–3430.

Chinnery, M. A., 1961. The deformation of the ground around surface faults. *Bull. seism. Soc. Am.*, **51,** 355–372.

Chinnery, M. A., 1964. The strength of the Earth's crust under horizontal shear stress, *J. geophys. Res.*, **69,** 2085–2089.

Chinnery, M. A., 1969. Earthquake magnitude and source parameters, *Bull. seism. Soc. Am.*, **59,** 1909–1982.

Karnik, V., Kondorskaya, N. V., Riznichenko, Ju. V., Saravensky, E. F., Soloviev, S. L., Shebalin, N. V., Vanek, J. & Zatopek, A., 1962. Standardisation of earthquake magnitude scale, *Studia Geophysica Geodetica*, **6,** 41–47.

Khattri, K. & Stauder, W., 1970. Kinematic parameters of five Rat Island earthquakes. (In press.)

Press, F., 1964. Long period waves and free oscillations of the earth, *Research in Geophysics*, 2, edited by H. Odishaw, M.I.T. Press, Cambridge, Mass.

Richter, C. R., 1958. *Elementary seismology*, W. H. Freeman & Co., San Francisco.

Stauder, W., 1960. *S* wave and focal mechanism: The state of the question; *Bull. seism. Soc. Am.* **50,** 333–346.

Stauder, W., 1968. Mechanism of the Rat Island earthquake sequence of February 4, 1965 with relation to island arcs and sea-floor spreading, *J. geophys. Res.*, **73,** 3948–3858.

Stauder, W. & Bollinger, G. A., 1966. The *S*-wave project for focal mechanism studies: Earthquakes of 1963, *Bull. seism. Soc. Am.*, **56,** 1363–1371.

Sykes, L. R., 1967. Mechanism of earthquake and nature of faulting on the mid-oceanic ridges, *J. geophys. Res.*, **72,** 2131–2153.

Udias, A. & Baumann, D., 1969. A computer program for focal mechanism determination combining *P* and *S* wave data, *Bull. seism. Soc. Am.*, **59,** 503–519.

Wyss, M. & Brune, J. N., 1968. Seismic moment, stress and source dimensions for earthquakes in the California–Nevada region, *J. geophys. Res.*, **73,** 4681–4684.